JOURNAL OF THERMOPHYSICS AND HEAT TRANSFER
Vol. 9, No. 3, July–September 1995

Computation of Hypersonic Flows with Finite Catalytic Walls

James H. Miller,* John C. Tannehill,† and Ganesh Wadawadigi‡
Iowa State University, Ames, Iowa 50011
and
Thomas A. Edwards§ and Scott L. Lawrence¶
NASA Ames Research Center, Moffett Field, California 94035

A computational study has been performed to explore the effects of finite catalytic walls on hypersonic flows. Boundary conditions for noncatalytic, fully catalytic, and finite catalytic walls have been incorporated into an upwind parabolized Navier–Stokes code. Nonequilibrium laminar airflows over sharp cones at 0 and 10 deg angle of attack were computed and the results are compared with previous results wherever possible. A study of finite catalytic cases was performed using varying recombination rates. Full ranges of catalycities were explored in the context of the surface energy balance as well as a constant wall temperature assumption. Detailed effects on specie concentrations, temperature, and heat transfer are presented.

Introduction

NONEQUILIBRIUM conditions exist in high-speed flows when the shock-body interaction causes the composition of the medium to change due to chemical reactions occurring at a finite rate.[1,2] For many such flight conditions, the recombination of atoms is dominant at the wall. The effect of the body surface on the recombination rates near the wall is described by the wall catalycity. The catalycity has two effects, the first is to increase the heat transfer and the second is to change the composition of the flow. Theoretically, the catalycity ranges from a fully catalytic condition to a noncatalytic one, although all surfaces will have a catalycity somewhere in-between. A fully catalytic wall will cause the recombination to occur instantaneously and the composition on the wall will be limited by the speed with which atoms diffuse to the wall. In this case, heat is released near the wall due to the exothermic recombination reactions. Usually the temperature gradient near the wall is large causing some of the energy to be absorbed into the wall. If the wall is noncatalytic, no recombination occurs at the wall and the resulting heat transfer can be much less. A finite catalytic wall is one that produces a situation between these two extremes.

The effects of catalytic walls on heat-transfer rates have been well known since the late 1950s.[3–5] In the early 1960s many of the published solutions considered only the fully catalytic boundary condition.[6,7] In the later 1960s and 1970s some work was performed to investigate the effects of both fully catalytic and noncatalytic walls.[8,9] Tong et al.[10] considered the effects of finite catalytic walls using the BLIMPK code in 1973. Presented in that study were heat transfer comparisons using average values for the catalycities of nitrogen, oxygen, and nitrogen oxide. It was noted by Scott[11] that these solutions can only be considered approximate and do not provide accurate information on the composition near the wall.

Subsequently, in the early 1980s, the work devoted to catalytic walls was mainly centered on the Space Shuttle flight experiments.[12–16] By comparing heat flux calculations with in-flight measurements it was inferred that chemical nonequilibrium existed.[17] The relatively noncatalytic nature of the Space Shuttle reaction-cured glass (RCG) tiles enabled investigators to easily verify the existence of in-flight nonequilibrium conditions. The catalytic surface effects experiment by Stewart et al.[13,18] helped to verify this and provided information on the catalycity of iron–cobalt–chromia spinel relative to the RCG tiles.

The emphasis on Space Shuttle calculations continued into the late 1980s and 1990s,[19] although some work has been performed to allow for catalytic effects on aerobraking-type vehicles.[20–22] For a space–plane configuration the effects of catalytic walls will be significant not only in terms of heat transfer, but also in terms of flowfield composition. The composition of the flow entering a hypersonic airbreathing engine will be paramount in accurately determining in-flight performance. The purpose of this study is to show some of the detailed effects of catalytic walls in terms of heat transfer and flowfield characteristics.

A modified version of the three-dimensional upwind parabolized Navier–Stokes (UPS) code of Lawrence et al.[23,24] has been used for the flow computations in this study. The UPS code solves the parabolized Navier–Stokes (PNS) equations using a finite volume, upwind method based on Roe's approximate Riemann solver.[25] It has been well-documented that the UPS code requires no user-specified smoothing terms that hindered many of the earlier centrally differenced PNS codes. The UPS code has previously been extended to permit equilibrium[26–28] and nonequilibrium[29,30] airflows as well as three-dimensional internal turbulent flows through scramjet engines with hydrogen–air chemistry.[31]

In the present study, the UPS code has been further extended to include a general finite catalytic wall boundary condition assuming either an isothermal wall or a more realistic condition defined by the surface energy balance. A full range of catalycity can be accommodated from noncatalytic to fully catalytic. The new code has been used to compute the $M_\infty = 25$ laminar flow of chemically reacting air over sharp cones at 0 and 10 deg angle of attack at an altitude of 61 km (200,000 ft). Additional calculations were performed for the $M_\infty = 22$

Presented as Paper 94-2354 at the AIAA 25th Fluid Dynamics Conference, Colorado Springs, CO, June 20–23, 1994; received July 11, 1994; revision received Dec. 2, 1994; accepted for publication Jan. 3, 1995.

*Graduate Teaching Assistant, Department of Aerospace Engineering and Engineering Mechanics. Student Member AIAA.

†Manager, Computational Fluid Dynamics Center and Professor, Department of Aerospace Engineering and Engineering Mechanics. Fellow AIAA.

‡Graduate Research Assistant; currently Research Associate, Center for Hypersonic Research, University of Texas, Arlington, TX. Member AIAA.

§Chief, Reacting Flow Environment Branch. Senior Member AIAA.

¶Research Scientist, Applied Computational Aerodynamics Branch. Member AIAA.

laminar flow over a sharp cone at 0 deg angle of attack at an altitude of 30.5 km (100,000 ft). Computations were performed for noncatalytic, fully catalytic, and finite catalytic cases, and the results are compared with previous results wherever possible.

Governing Equations

The PNS equations are obtained from the compressible Navier–Stokes equations by neglecting the streamwise viscous terms and dropping the unsteady terms. Vigneron's technique,[32] which was extended by Prabhu et al.[33] for nonequilibrium flows, is used to eliminate the ellipticity in the marching direction due to the streamwise pressure gradient. The PNS equations expressed in a general nonorthogonal coordinate system ξ, η, ζ are given by

$$\boldsymbol{E}_\xi + \boldsymbol{F}_\eta + \boldsymbol{G}_\zeta = 0 \tag{1}$$

where

$$\begin{aligned} \boldsymbol{E} &= (\xi_x/J)\boldsymbol{E}_i + (\xi_y/J)\boldsymbol{F}_i + (\xi_z/J)\boldsymbol{G}_i \\ \boldsymbol{F} &= (\eta_x/J)(\boldsymbol{E}_i - \boldsymbol{E}_v^*) + (\eta_y/J)(\boldsymbol{F}_i - \boldsymbol{F}_v^*) \\ &\quad + (\eta_z/J)(\boldsymbol{G}_i - \boldsymbol{G}_v^*) \\ \boldsymbol{G} &= (\zeta_x/J)(\boldsymbol{E}_i - \boldsymbol{E}_v^*) + (\zeta_y/J)(\boldsymbol{F}_i - \boldsymbol{F}_v^*) \\ &\quad + (\zeta_z/J)(\boldsymbol{G}_i - \boldsymbol{G}_v^*) \end{aligned} \tag{2}$$

The inviscid and viscous flux vectors are given by

$$\begin{aligned} \boldsymbol{E}_i &= \{\rho u,\ \rho u^2 + p,\ \rho uv,\ \rho uw,\ (E_t + p)u\}^T \\ \boldsymbol{F}_i &= \{\rho v,\ \rho uv,\ \rho v^2 + p,\ \rho vw,\ (E_t + p)v\}^T \\ \boldsymbol{G}_i &= \{\rho w,\ \rho uw,\ \rho vw,\ \rho w^2 + p,\ (E_t + p)w\}^T \\ \boldsymbol{E}_v &= \{0,\ \tau_{xx},\ \tau_{xy},\ \tau_{xz},\ u\tau_{xx} + v\tau_{xy} + w\tau_{xz} - q_x\}^T \\ \boldsymbol{F}_v &= \{0,\ \tau_{yx},\ \tau_{yy},\ \tau_{yz},\ u\tau_{yx} + v\tau_{yy} + w\tau_{yz} - q_y\}^T \\ \boldsymbol{G}_v &= \{0,\ \tau_{zx},\ \tau_{zy},\ \tau_{zz},\ u\tau_{zx} + v\tau_{zy} + w\tau_{zz} - q_z\}^T \end{aligned} \tag{3}$$

where $E_t = \rho\{e + \frac{1}{2}(u^2 + v^2 + w^2)\}$. The superscript asterisks on the viscous flux vectors in Eq. (2) indicate that the derivatives with respect to ξ have been dropped. In the previous equations, p is the pressure; ρ is the density; u, v, and w are the velocity components in the x, y, and z directions, respectively; e is the internal energy; τ is the viscous stress; and q is the heat conduction rate.

For nonequilibrium flows the species continuity equations must be solved in addition to the fluid equations. Using the global continuity equation and assuming Fick's law for mass diffusion, the steady form of the species continuity equation is written

$$\rho \boldsymbol{V}\cdot\nabla c_s = \nabla\cdot(\rho D_{sm}\nabla c_s) + \dot{\omega}_s \qquad s = 1, 2, \ldots, n \tag{4}$$

where c_s is the species mass fraction, D_{sm} is the multicomponent diffusion coefficient, and $\dot{\omega}_s$ is the mass production/depletion rate of species s. In the present study, a binary diffusion coefficient D is used and is assumed to be the same for all the species. The species continuity equations are simplified using the PNS assumption of dropping the streamwise diffusion terms. The effect of mass diffusion of species in the energy equation is accounted for by adding the following component to the heat flux terms (q_x, q_y, q_z):

$$\rho \sum_{s=1}^{n} c_s U_s h_s \tag{5}$$

where U_s is the diffusion velocity of species s and h_s is the species enthalpy.

The species enthalpy, specific heat, and viscosity are obtained from a table-look-up procedure using the data of Ref. 34. The species thermal conductivity is computed using Eucken's semiempirical formula. The viscosity and thermal conductivity of the mixture are calculated using Wilke's semiempirical mixing rule,[35] and the binary Lewis number Le is assumed to be the same constant for all the species. The chemistry model used in this study is that of air consisting of seven species ($n = 7$), including electrons and seven reactions ($m = 7$). This model is identical to that used by Blottner et al.[34] and Prabhu et al.[36] The constituent species are molecular oxygen (O_2), atomic oxygen (O), atomic nitrogen (N), nitric oxide (NO), nitric oxide ion (NO^+), molecular nitrogen (N_2), and electrons (e^-). The following reactions are considered:

$$\begin{aligned} O_2 + M_1 &\rightleftharpoons 2O + M_1 \\ N_2 + M_2 &\rightleftharpoons 2N + M_2 \\ N_2 + N &\rightleftharpoons 2N + N \\ NO + M_3 &\rightleftharpoons N + O + M_3 \\ NO + O &\rightleftharpoons O_2 + N \\ N_2 + O &\rightleftharpoons NO + N \\ N + O &\rightleftharpoons NO^+ + e^- \end{aligned} \tag{6}$$

The reaction rates are obtained from Ref. 34.

Numerical Method

A finite volume, upwind, total variation diminishing (TVD) scheme is used to integrate the fluid equations. The algorithm is second-order accurate in the crossflow plane and first-order accurate in the streamwise marching direction. The upwind algorithm is based on Roe's steady approximate Riemann solver,[25] which has been modified[29] for nonequilibrium effects. Second-order central differences are used to model the viscous terms.

The species continuity equations are solved using a finite volume approach. The requirement that the mass fraction of the species sum to unity eliminates the nth species continuity equation. This results in requiring only $n - 1$ equations to be solved. The convective terms are modeled using first-order upwind differences in a conservative manner. The species production/depletion rate $\dot{\omega}_s$ is treated as a source term and is lagged to the nth marching station for the present calculations. A line Gauss–Seidel procedure with successive overrelaxation (SOR), in conjunction with a scalar tridiagonal solver for each line, is employed to solve each equation.

The coupling between the fluids and chemistry is achieved in a "loosely coupled" manner. First the fluid equations are solved assuming no change in the composition. The new density and velocity are then used in the solution of the species continuity equations. Once the species mass fractions are found, the new density, internal energy, temperature, pressure, and specific heats are determined. The coupling between the fluids and chemistry can be enhanced through the implementation of Newton iterations on the governing equations at each streamwise step.[30] However, this was found not to be necessary for the cases considered in this study. Further details of the algorithm can be found in Refs. 23, 24, and 26–31.

Finite Catalytic Wall Boundary Condition

The boundary condition for a finite catalytic wall is discussed in detail by Anderson,[1] Park,[2] Scott [Refs. 37 and 17 (pp. 394–400)], Bruno,[38] and Goulard.[3] Following the derivation given by Scott,[37] the expression for the boundary condition at a finite catalytic wall for a given species can be written as

$$D\left(\frac{\partial c_s}{\partial n}\right)_{\text{wall}} = K_s c_s \qquad s = 1, 2, \ldots, n \tag{7}$$

where D is the binary diffusion coefficient, K_s is the catalytic recombination rate for the species, and n is the coordinate normal to the wall. All of the above quantities are evaluated at the wall. Scott has shown that the recombination rate can be related to the recombination coefficient γ_s through the following equation:

$$K_s = \gamma_s \sqrt{(kT/2\pi)(N_{av}/M_s)} \tag{8}$$

where γ_s is defined as the fraction of atoms impinging on the surface that recombine. In this equation k is the Boltzmann constant, M_s is the molecular weight of the species, N_{av} is Avogadro's number, and T is the temperature in degrees Kelvin.

The recombinations of nitrogen, oxygen, and nitrogen oxide have been accepted by many investigators to be the most important reactions occurring on a finite catalytic wall,[38,39] with the nitrogen oxide recombination being less important than the other two. The nitrogen oxide recombination reaction has been ignored in this study. This leaves the following reactions at the wall:

$$\begin{aligned} N + N &\rightarrow N_2 \\ O + O &\rightarrow O_2 \end{aligned} \tag{9}$$

For this study, a fully catalytic wall is defined as $\gamma_N = \gamma_0 = 1$. Another interpretation[40] for a fully catalytic wall is to assume the species concentrations at the wall are equal to their equilibrium concentrations based on the local temperature and pressure. For wall temperatures below 2000 K (so-called "cold walls"), this corresponds to the composition of the ambient air. In this study it will be shown that these two interpretations are reasonably consistent with each other for a constant wall-temperature, cold-wall flow test case. In general, these two interpretations will produce different results. A noncatalytic wall is defined by setting γ_s to zero.

As discussed in Ref. 41, the species continuity equations are solved for each species using a scalar tridiagonal solver. The species mass fractions at the point $L = 1$ (see Fig. 1) must be written in terms of the mass fractions at $L = 2$ to incorporate the boundary condition [Eq. (7)] into the implicit system of equations. Using a differenced form of Eq. (7), the species mass fractions at point $L = 1$ are determined from

$$(c_s)_1 = (c_s)_2 - (K_s \Delta n/D)(c_s)_{wall} \tag{10}$$

where K_s is evaluated at the previous marching station and $(c_s)_{wall}$ is approximated by

$$(c_s)_{wall} = \frac{(c_s)_1 + (c_s)_2}{2} \tag{11}$$

For a noncatalytic wall, $K_s = 0$, which reduces Eq. (10) to

$$(c_s)_1 = (c_s)_2 \tag{12}$$

For a fully catalytic wall, K_s is calculated with $\gamma_s = 1$.

In the case of a finite catalytic wall, Eq. (7) is employed for the atomic nitrogen and atomic oxygen species. The nitrogen oxide and nitrogen oxide ion species are treated as noncatalytic. The mass fraction of molecular nitrogen (N_2) is obtained by utilizing the fact that all mass fractions sum to unity. For molecular oxygen (O_2), the gradient must be implemented such that oxygen atoms are conserved at the wall. This is accomplished with the equation:

$$\left.\frac{\partial c_{O_2}}{\partial n}\right)_{wall} = -\left.\frac{\partial c_O}{\partial n}\right)_{wall} \tag{13}$$

where the gradient for atomic oxygen is determined from Eq. (7).

In this study, the γ_s values are treated as constants and not functions of temperature. This assumption is made because of the lack of theoretical and experimental data to provide accurate correlations between γ_s and wall temperature for materials other than those used on the Space Shuttle.[42-44]

Surface Energy Balance for Finite Catalytic Walls

The previous description of the finite catalytic boundary condition is based on the principle of conservation of mass applied at the wall. In most hypersonic flows the surface energy balance must also be employed to accurately determine the heat transfer rates and detailed characteristics of the flowfield. This important aspect is often neglected in the literature where it is usually assumed that the vehicle surface can maintain a constant wall temperature regardless of the flowfield. Only in rare instances is this a fair approximation.

The surface energy balance in this study takes the following form:

$$q_w = \kappa \frac{\partial T}{\partial n} + \sum_{s=1}^{n} h_s \rho D \frac{\partial c_s}{\partial n} = \varepsilon \sigma (T)^4 \tag{14}$$

where the emissivity ε is taken as a constant equal to 0.85, and σ is the Stefan–Boltzmann constant. This equation assumes that the surface is at radiative equilibrium and there is no radiation contribution from the flow to the wall and no conduction loss through the wall. In the present study the wall temperature is updated explicitly at each streamwise station using a Newton–Raphson approach. Convergence is usually achieved within 7–10 iterations.

Numerical Results

Test Case 1

The geometry for test case 1 consists of a sharp cone with a length of 0.5 m and cone half-angles of 10 and 20 deg. The coordinate system is shown in Fig. 2. The flow conditions for this test case are identical to those of Prabhu[36] and Molvik and Merkle.[45] The velocity and altitude are 8071 m/s and 60.96 km, respectively. This particular flight condition corresponds to the expected maximum cruise Mach number of a space-plane prior to the rocket-assisted ascent into orbit. The free-stream temperature and pressure at this altitude are 252.6 K and 20.35 N/m^2, respectively. These conditions result in a Mach number of 25.32 and a Reynolds number of 1.28777 $\times$ 10^5/m. The composition of the air was assumed to be 26.29%

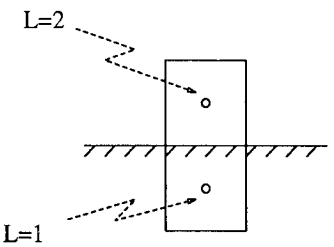

Fig. 1 Finite volume geometry at the wall.

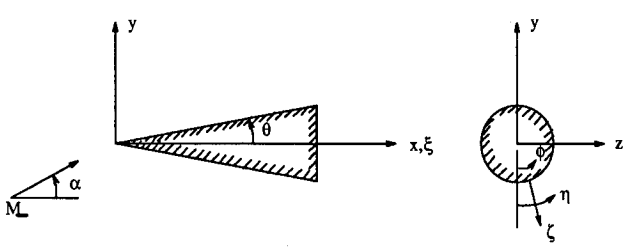

Fig. 2 Coordinate system.

molecular oxygen and 73.71% molecular nitrogen, where the percentages are in terms of mass. The Lewis number was held constant equal to 1.4. Two approaches were used to implement the boundary conditions. In one approach the wall temperature was fixed at 1200 K and in the other, the surface energy balance was used to determine the wall temperature at each station. All test cases throughout this study were started with an initial solution obtained using a conical stepback procedure.[46]

The first set of calculations were for a 10-deg cone at 0 deg angle of attack with either constant wall temperature or surface energy balance boundary conditions. The grid contained 50 cells in the normal (radial) direction and 14 cells in the circumferential direction. A grid refinement study was performed using 75 and 20 cells, respectively, and the change in computed results was negligible.

These calculations were started at an initial station of x = 0.01 m. The height of the first cell next to the wall was held fixed at 1.0×10^{-4} m for the constant wall temperature approach and 1.0×10^{-5} m for the surface energy balance approach. The outer grid height varied in the streamwise direction with the outer grid angle set to 20 and 15 deg, respectively. The wall spacing and grid height were used to determine the appropriate Roberts' stretching parameter[46] for the remaining cells (points). The average number of steps taken (including stepback) for the fully catalytic cases was 4000 for the constant wall temperature approach and 2500 for the surface energy balance approach. In general, the noncatalytic assumption required fewer steps (approximately half). The number of steps used for intermediate ranges of catalycity were between the fully catalytic and noncatalytic values.

The species profiles of O and NO at the end of the cone for the constant wall temperature boundary condition are shown in Figs. 3 and 4, respectively. The noncatalytic case is compared with the results of Buelow et al.[47] The small difference in results relative to Ref. 47 are due to different starting solutions. The starting solution in Ref. 47 consisted of an impulsive start as opposed to the conical stepback procedure used in the present study. The two different interpretations for the fully catalytic wall give similar results for the O profile, but different results for the NO profile. The two definitions appear to be somewhat consistent for this particular test case, although the two definitions represent distinctly different physical interpretations.

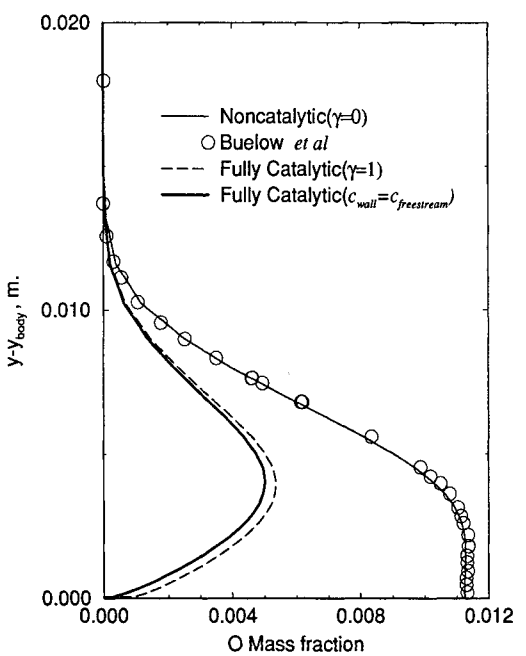

Fig. 3 O profiles at x = 0.5 m (α = 0, θ = 10, T_{wall} = 1200 K).

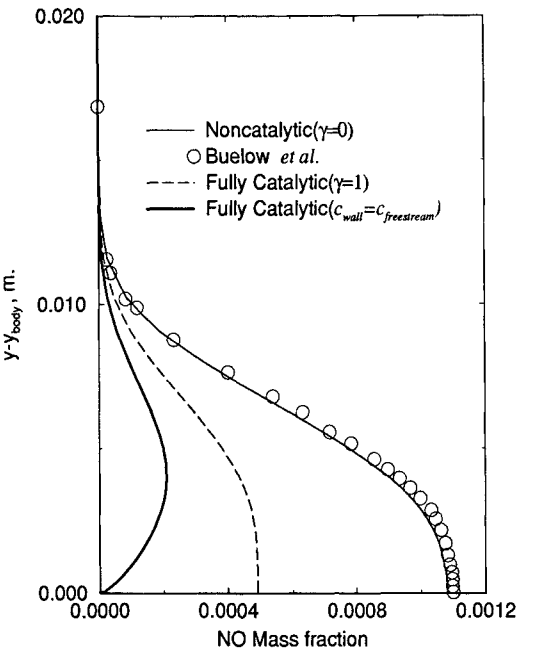

Fig. 4 NO profiles at x = 0.5 m (α = 0, θ = 10, T_{wall} = 1200 K).

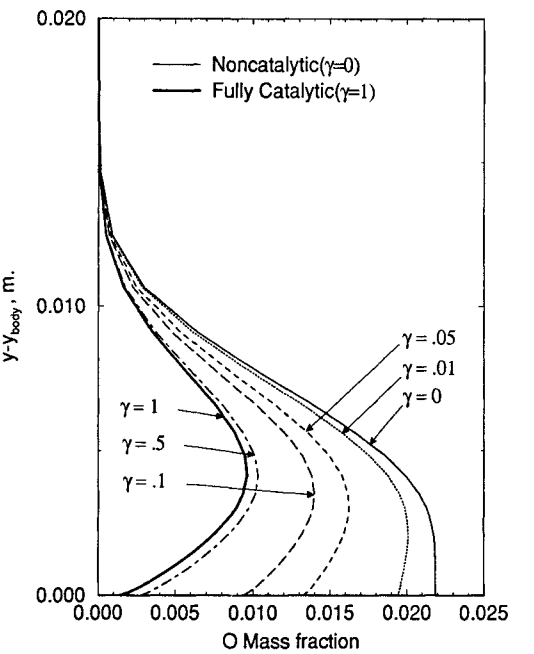

Fig. 5 O profiles at x = 0.5 m (α = 0, θ = 10, surface energy boundary condition).

The surface energy balance boundary condition was then implemented for this case. The species profiles of O and NO are shown in Figs. 5 and 6, respectively. These results are similar in shape to those in Figs. 3 and 4, although the magnitudes of the species mass fractions are much higher due to the higher temperatures present in the flow.

In the next calculation, the cone half-angle was increased from 10 to 20 deg. The freestream conditions and the number of points in the radial and circumferential directions were kept the same. The outer grid angle was set to 25 deg and the height of the first cell above the wall was fixed at 5.0×10^{-6} m. Calculations started at an initial station of x = 0.01 m, as before, and the surface energy balance was used to determine the wall temperature at each x station. The species profile shapes for O are presented in Fig. 7. As expected, the magnitude of the atomic oxygen mass fractions are significantly

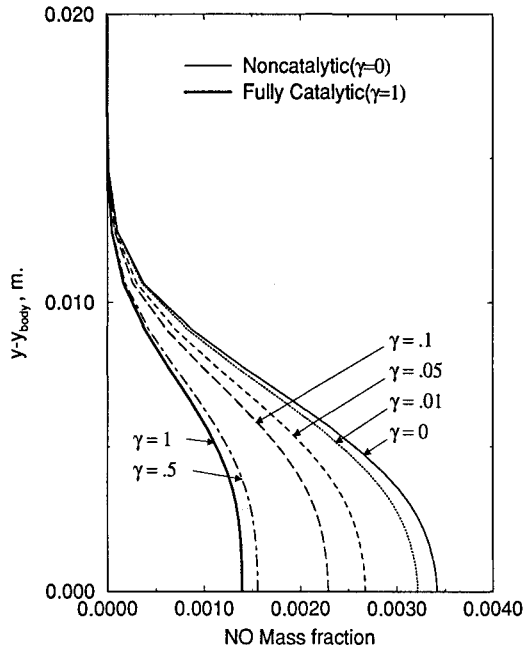

Fig. 6 NO profiles at $x = 0.5$ m ($\alpha = 0$, $\theta = 10$, surface energy boundary condition).

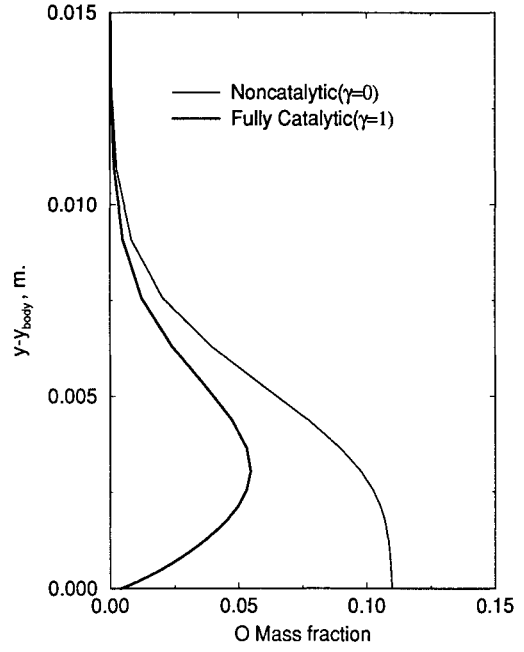

Fig. 7 O profiles at $x = 0.5$ m ($\alpha = 0$, $\theta = 20$, surface energy boundary condition).

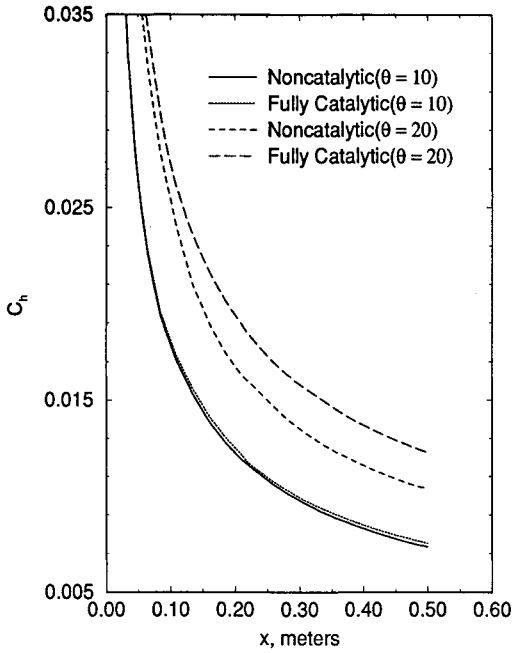

Fig. 8 Heat transfer effects ($\alpha = 0$, $\theta = 10$, 20, surface energy boundary condition).

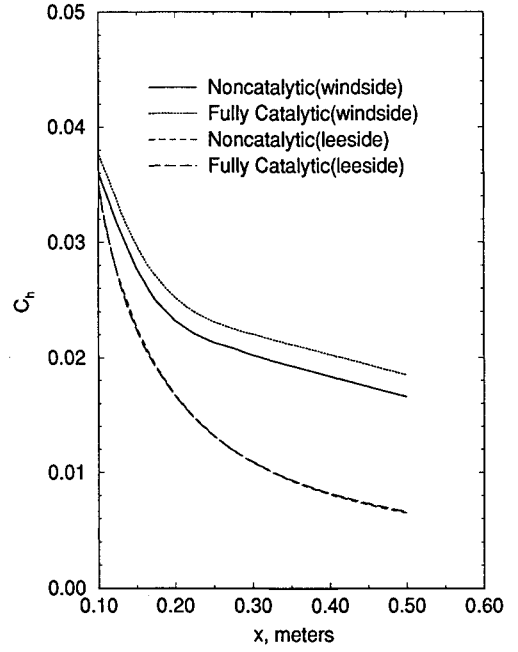

Fig. 9 O profiles at $x = 0.5$ m ($\alpha = 10$, $\theta = 10$, surface energy boundary condition).

higher when the cone angle is increased to 20 deg. The heat transfer results are presented in Fig. 8 for the noncatalytic and fully catalytic cases. Included in this graph are the results for the 10-deg cone. For the 20-deg case, the increase in heat transfer due to catalycity is about 20% and is negligible for the 10-deg case. The increase in heat transfer due to the cone half-angle is more significant. Figure 8 shows a 70% increase in heat transfer between the 10- and 20-deg fully catalytic cone cases. It is clear that the change in heat transfer due to catalycity is very sensitive to the strength of the shock. For cone angles greater than 20 deg, it was necessary to reduce the safety factor on Vigneron's parameter for a fully catalytic boundary condition. The factor was reduced from 0.95 to approximately 0.55. For a noncatalytic case no reduction was required.

In the next calculation, the angle of attack of the 10-deg half-angle cone was increased to 10 deg and the surface energy balance was used to determine the wall temperature at each station. The number of points was kept at 50 in the radial direction, but was increased to 30 in the circumferential direction. The height of the first cell above the wall was fixed at 5.0×10^{-5} m for the lee-side and 1.0×10^{-5} m for the wind-side. Calculations were started at an initial station of $x = 0.05$ m. The outer grid height varied in the streamwise direction with the outer grid angle set to 35 deg for the lee-side and 15 deg for the wind-side. The heat transfer coefficients are shown in Fig. 9. The increase in heat transfer due to wall catalycity on the wind-side is much more significant than on the lee-side. These results show the effect of a stronger shock on the wind-side when compared to the lee-side. Figure

10 shows the effect on the atomic oxygen mass fraction due to catalycity on the wind-side and lee-side.

Test Case 2

In this test case the flight conditions correspond to calculations performed by Blottner[6] in 1964. This reference is one of the few to show results for a fully catalytic sharp cone case. The cone half-angle for this case is 10 deg. The flight conditions given by Blottner are a freestream velocity of 22,000 ft/s (6706 m/s) and an altitude of 100,000 ft (30.48 km). The corresponding boundary-layer edge conditions are u_e = 21,590 ft/s (6581 m/s), T_e = 1019 K, and p_e = 522.6 lb/ft^2 (25,022 N/m^2). The input for the UPS code requires only freestream quantities and these were varied until the UPS boundary-layer edge conditions were approximately the same as given by Blottner. The final freestream conditions used were M_∞ = 22.1, $Re_\infty = 6.763 \times 10^6$, and T_∞ = 232.7 K. The freestream mass fractions were 0.2328 for O_2 and 0.7672 for N_2.

The fully catalytic definition used for this test case is based on the cold-wall assumption where the mass fractions at the wall are set to their freestream values. This approach was used to approximately match Blottner's calculations where the wall mass fractions were determined from the equilibrium composition based on the temperature and pressure at the edge of the boundary layer.

The grid used for these calculations is similar to the previous test case. The outer grid angle was set to 20 deg and the number of radial points was 100. The height of the first cell at the wall was 1.0×10^{-5} m. The starting solution was obtained as in the previous test case and the calculations proceeded until an x station of 11.02 ft (3.36 m) was reached.

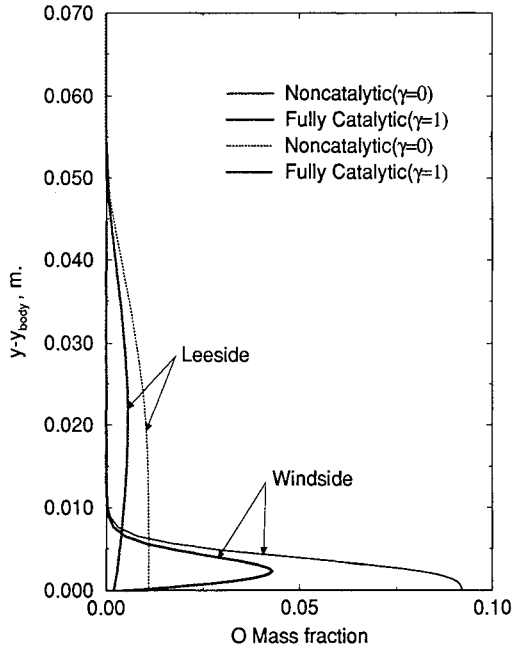

Fig. 10 Heat transfer effects (α = 10, θ = 10, surface energy boundary condition).

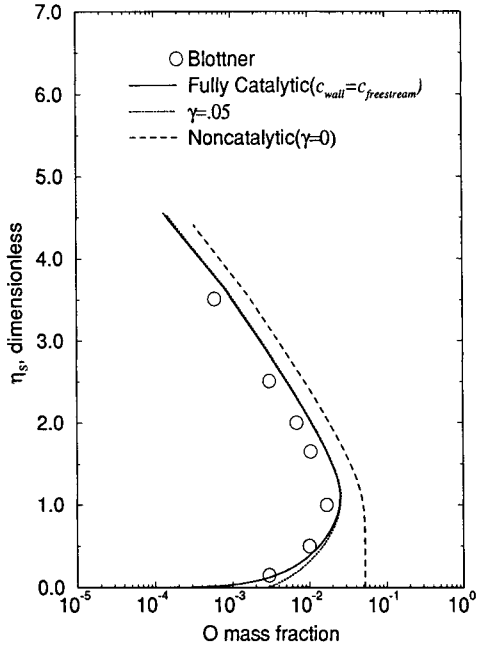

Fig. 11 O profiles at x = 11.02 ft (α = 0, θ = 10, T_{wall} = 1000 K).

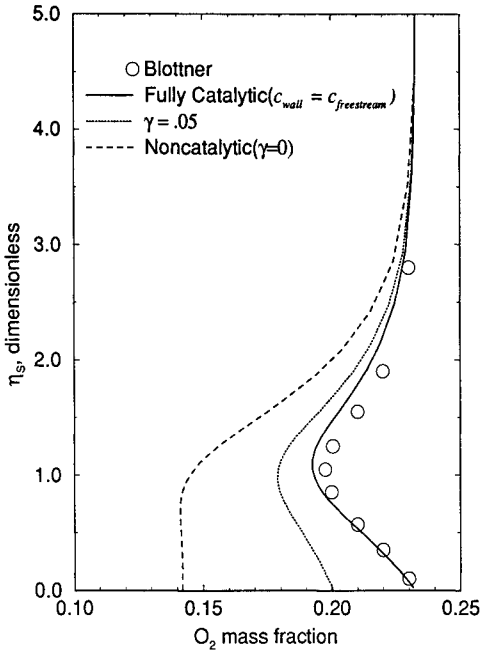

Fig. 12 O_2 profiles at x = 11.02 ft (α = 0, θ = 10, T_{wall} = 1000 K).

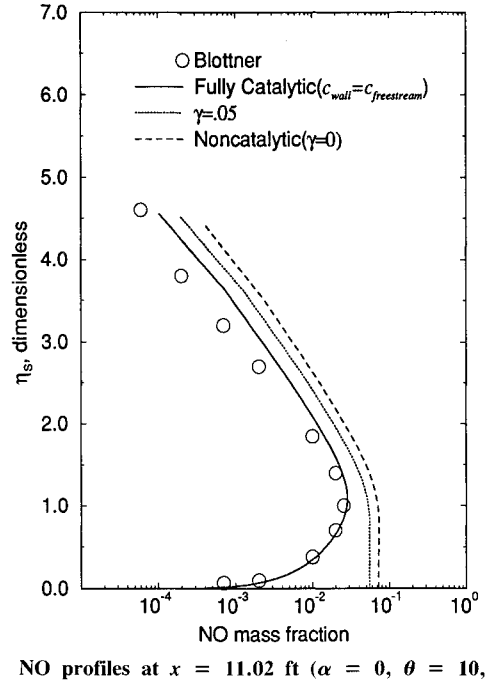

Fig. 13 NO profiles at x = 11.02 ft (α = 0, θ = 10, T_{wall} = 1000 K).

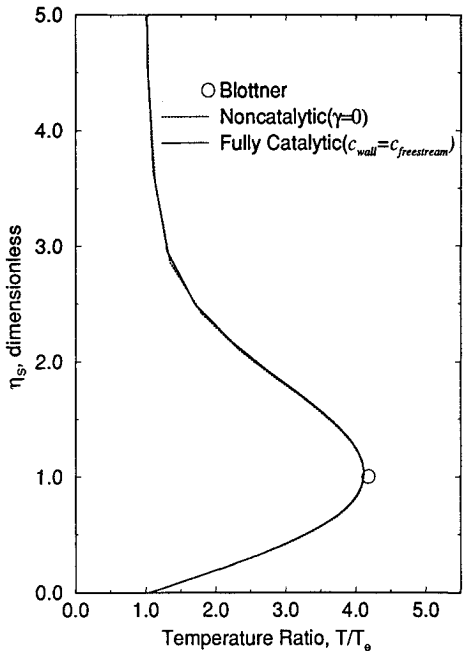

Fig. 14 Temperature profiles at x = 11.02 ft (α = 0, θ = 10, T_{wall} = 1000 K).

The y coordinate used in Ref. 6 is given in terms of the similarity variable η_s. For convenience, the similarity variables employed in Ref. 6 are repeated here:

$$\xi_s(x) = \int_0^x (\rho\mu)_e u_e r_b^2 \, dx$$
$$\eta_s(x, y) = \frac{u_e r_b}{(2\xi_s)^{1/2}} \int_0^y \rho \, dy \tag{15}$$

Figure 11 shows the atomic oxygen profiles at an x station of 11.02 ft. The noncatalytic and fully catalytic solutions are shown in addition to a finite catalytic calculation. The fully catalytic solutions are in reasonable agreement. The difference in results is believed to be due to the differences in edge conditions and in the equations being solved. The solutions presented in Ref. 6 were obtained from the boundary-layer equations that were coupled with a system of ordinary differential equations that described the inviscid portion of the shock layer.

Figures 12 and 13 show the molecular oxygen and nitrogen oxide profiles. Good agreement is obtained for the fully catalytic solutions, although the NO profile given by Blottner asymptotically reaches a value of about 5×10^{-5} and the UPS solution reaches a value very near zero when the similarity variable η_s reaches a value greater than 5. This is due to the slight difference in fully catalytic interpretations as mentioned previously. The temperature profile is shown in Fig. 14. The temperature profile is not given for this x station in Ref. 6, but the peak temperature is given and its value compares well with the peak value computed in the present computation.

Concluding Remarks

The three-dimensional UPS code has been extended to allow for finite rate catalytic walls. Nonequilibrium laminar airflows over sharp cones at zero and 10 deg angle of attack were computed using noncatalytic, fully catalytic, and finite catalytic wall boundary conditions. These boundary conditions were based on either a surface energy balance or a constant wall temperature assumption. The effects of these boundary conditions on species concentrations, temperature, and heat transfer were studied and compared with previously computed noncatalytic and fully catalytic cases. Large differences in results were found between the surface energy balance and the constant wall temperature boundary condition. The effects of catalycity on heat transfer and flow composition were found to be very sensitive to the strength of the shock resulting from different cone half-angles or angles of attack. Additional results are given in Ref. 41.

Acknowledgments

This work was supported by NASA Ames Research Center under Grant NAG 2-776. The Technical Monitors for this grant have been Thomas A. Edwards and Scott L. Lawrence.

References

[1]Anderson, J. D., Jr., "Hypersonics and High Temperature Gas Dynamics," McGraw-Hill, New York, 1989, pp. 623–626.

[2]Park, C., "Nonequilibrium Hypersonic Aerothermodynamics," Wiley, New York, 1990, p. 142.

[3]Goulard, R., "On Catalytic Recombination Rates in Hypersonic Stagnation Heat Transfer," *Jet Propulsion*, Vol. 28, Nov. 1958, pp. 737–745.

[4]Fay, A. J., and Ridell, F. R., "Theory of Stagnation Point Heat Transfer in Dissociated Air," *Journal of the Aeronautical Sciences*, Vol. 28, Feb. 1958, pp. 73–122.

[5]Inger, G. R., "Nonequilibrium Stagnation Point Boundary Layers with Arbitrary Surface Catalycity," *AIAA Journal*, Vol. 1, No. 8, 1963, pp. 1776–1784.

[6]Blottner, F. G., "Nonequilibrium Laminar Boundary Layer Flow of Ionized Air," *AIAA Journal*, Vol. 2, No. 11, 1964, pp. 1921–1927.

[7]Levinsky, E. S., and Fernandez, F. L., "Approximate Non-Equilibrium, Air Ionization in Hypersonic Flows over Sharp Cones," *AIAA Journal*, Vol. 2, No. 3, 1964, pp. 565–568.

[8]Blottner, F. G., "Electron Number Density Distribution in the Laminar Air Boundary Layer on Sharp Cones," *AIAA Journal*, Vol. 7, No. 6, 1969, pp. 1064–1069.

[9]Oyegbesan, A. O., and Algermissen, J., "Non-Equilibrium Laminar Boundary-Layer Flow of Dissociating Air," *ACTA Astronautica*, Vol. 3, Nos. 5–6, 1976, pp. 377–394.

[10]Tong, H., Buckingham, A. C., and Morse, H. L., "Nonequilibrium Chemistry Boundary Layer Integral Matrix Procedure," Acurex Corp., NASA-CR-134039, 1973.

[11]Scott, C. D., "Space Shuttle Laminar Heating with Finite Rate Catalytic Recombination," AIAA Paper 81-1144, June 1981.

[12]Scott, C. D., "Space Shuttle Laminar Heating with Finite-Rate Catalytic Recombination," *Thermophysics of Atmospheric Entry*, edited by T. E. Horton, Vol. 82, Progress in Astronautics and Aeronautics, AIAA, New York, 1982, pp. 273–289.

[13]Stewart, D. A., Rakich, J. V., and Lanfranco, M. J., "Catalytic Surface Effects Experiment on the Space Shuttle," *Thermophysics of Atmospheric Entry*, edited by T. E. Horton, Vol. 82, Progress in Astronautics and Aeronautics, AIAA, New York, 1982, pp. 248–272.

[14]Rakich, J. V., Stewart, D. A., and Lanfranco, M. J., "Results of a Flight Experiment on the Catalytic Efficiency of the Space Shuttle Heat Shield," AIAA Paper 82-0944, June 1982.

[15]Gupta, R. N., Moss, J. N., Simmonds, A. L., Shinn, J. L., and Zoby, E. V., "Space Shuttle Heating Analysis with Variation in Angle of Attack and Surface Condition," AIAA Paper 83-0486, Jan. 1983.

[16]Gupta, R. N., Moss, J. N., Simmonds, A. L., Shinn, J. L., and Zoby, E. V., "Space Shuttle Heating Analysis with Variation in Angle of Attack and Catalycity," *Journal of Spacecraft and Rockets*, Vol. 21, No. 2, 1984, pp. 217–219.

[17]Scott, C. D., "Effects of Thermochemistry, Nonequilibrium and Surface Catalysis on the Design of Hypersonic Vehicles," *Hypersonics—Defining the Hypersonic Environment*, Vol. 1, Birhäuser, Boston, 1989, pp. 355–427.

[18]Stewart, D. A., Rakich, J. V., Lanfranco, M. J., and Scott, C. D., "Catalytic Surface Effects Experiment on Space Shuttle Thermal Protection System During Earth Entry of Flights STS-2 Through STS-5," NASA CP-2283, Pt. 2, March 1983, pp. 827–845.

[19]Kleb, W. L., and Weilmuenster, K. J., "Characteristics of the Shuttle Orbiter Leeside Flow During a Reentry Condition," AIAA Paper 92-2951, July 1992.

[20]Rochelle, W. C., Ting, P. C., Bouslog, S. A., Mueller, S. R., Colovin, J. E., Jr., Curry, D. M., and Scott, C. D., "Aeroassist Flight Experiment Heating-Rate Sensitivity Study," *Journal of Ther-*

mophysics, Vol. 4, No. 4, 1991, pp. 456–462.

[21]Stewart, D. A., Chen, Y.-K., and Henline, W. D., "Effect of Non-Equilibrium Flow Chemistry and Surface Catalysis on Surface Heating to AFE," AIAA Paper 91-1373, June 1991.

[22]Stewart, D. A., Henline, W. D., Kolodziej, P., and Pincha, E. M. W., "Effect of Surface Catalysis on Heating to Ceramic Coated Thermal Protection Systems for Transatmospheric Vehicles," AIAA Paper 88-2706, June 1988.

[23]Lawrence, S. L., Tannehill, J. C., and Chaussee, D. S., "Upwind Algorithm for the Parabolized Navier-Stokes Equations," *AIAA Journal*, Vol. 27, No. 9, 1989, pp. 1175–1183.

[24]Lawrence, S. L., Chaussee, D. S., and Tannehill, J. C., "Application of an Upwind Algorithm to the Three-Dimensional Parabolized Navier-Stokes Equations," *AIAA Journal*, Vol. 28, No. 6, 1990, pp. 971, 972.

[25]Roe, P. L., "Approximate Riemann Solvers, Parameters, Vectors, and Difference Schemes," *Journal of Computational Physics*, Vol. 43, No. 2, 1983, pp. 357–372.

[26]Tannehill, J. C., Ievalts, J. O., and Lawrence, S. L., "An Upwind Parabolized Navier-Stokes Code for Real Gas Flows," AIAA Paper 88-0713, Jan. 1988.

[27]Tannehill, J. C., Ievalts, J. O., and Lawrence, S. L., "A Three-Dimensional Upwind Parabolized Navier-Stokes Code for Real Gas Flows," AIAA Paper 89-1651, June 1989.

[28]Tannehill, J. C., Buelow, P. E., Ievalts, J. O., and Lawrence, S. L., "Three-Dimensional Upwind Parabolized Navier-Stokes Code for Real Gas Flows," *Journal of Spacecraft and Rockets*, Vol. 27, No. 2, 1990, pp. 150–159.

[29]Tannehill, J. C., Ievalts, J. O., Buelow, P. E., Prabhu, D. K., and Lawrence, S. L., "Upwind Parabolized Navier-Stokes Code for Chemically Reacting Flows," *Journal of Thermophysics and Heat Transfer*, Vol. 4, No. 2, 1990, pp. 149–156.

[30]Buelow, P. E., Tannehill, J. C., Ievalts, J. O., and Lawrence, S. L., "A Three-Dimensional, Upwind, Parabolized Navier-Stokes Code for Chemically Reacting Flows," *Journal of Thermophysics and Heat Transfer*, Vol. 5, No. 3, 1991, pp. 274–283.

[31]Wadawadigi, G., Tannehill, J. C., Buelow, P. E., and Lawrence, S. L., "A Three-Dimensional Upwind PNS Code for Chemically Reacting Scramjet Flowfields," AIAA Paper 92-2898, July 1992.

[32]Vigneron, Y. C., Rakich, J. V., and Tannehill, J. C., "Calculation of Supersonic Flow over Delta Wings with Sharp Subsonic Leading Edges," AIAA Paper 78-1137, July 1978.

[33]Prabhu, D. K., Tannehill, J. C., and Marvin, J. G., "A New PNS Code for Chemical Nonequilibrium," *AIAA Journal*, Vol. 26, No. 7, 1988, pp. 808–815.

[34]Blottner, F. G., Johnson, M., and Ellis, M., "Chemically Reacting Viscous Flow Program for Multi-Component Gas Mixtures," Sandia Labs., Rept. SC-RR-70-754, Albuquerque, NM, Dec. 1971.

[35]Wilke, C. R., "A Viscosity Equation for Gas Mixtures," *Journal of Chemical Physics*, Vol. 18, No. 4, 1950, p. 517.

[36]Prabhu, D. K., Tannehill, J. C., and Marvin, J. G., "A New PNS Code for Three-Dimensional Chemically Reacting Flows," AIAA Paper 87-1472, June 1987.

[37]Scott, C. D., "Wall Boundary Equations with Slip and Catalysis for Multicomponent Nonequilibrium Gas Flows," NASA-TMX-58111, Dec. 1973.

[38]Bruno, C., "Modeling Catalytic Recombination Heating at High Speed," AIAA Paper 89-0309, Jan. 1989.

[39]Milos, F. S., and Rasky, D. J., "Numerical Procedures for Three-Dimensional Computational Surface Thermochemistry," AIAA Paper 92-2944, July 1992.

[40]Grumet, A. A., Anderson, J. D., Jr., and Lewis, M. J., "A Numerical Study of Shock Wave/Boundary Layer Interaction in Nonequilibrium Chemically Reacting Air: The Effects of Catalytic Walls," AIAA Paper 91-0245, Jan. 1991.

[41]Miller, J. H., Tannehill, J. C., Wadawadigi, G., Edwards, T. A., and Lawrence, S. L., "Computation of Hypersonic Flows with Finite-Catalytic Walls," AIAA Paper 94-2354, June 1994.

[42]Jumper, E. J., Newman, M., and Seward, W. A., "Recombination of Nitrogen on Silica-Based Thermal-Protection-Tile-Like Surfaces," AIAA Paper 93-0477, Jan. 1993.

[43]Seward, W. A., and Jumper, E. J., "Model for Oxygen Recombination on Silicon-Dioxide Surfaces," *Journal of Thermophysics and Heat Transfer*, Vol. 5, No. 3, 1991, pp. 284–291.

[44]Willey, R. J., "Comparison of Kinetic Models for Atom Recombination High Temperature Reusable Surface Insulation," *Journal of Thermophysics and Heat Transfer*, Vol. 7, No. 1, 1993, pp. 55–62.

[45]Molvik, G. A., and Merkle, C. L., "A Set of Strongly-Coupled Upwind Algorithms for Computing Flows in Chemical Nonequilibrium," AIAA Paper 89-0199, Jan. 1989.

[46]Anderson, D. A., Tannehill, J. C., and Pletcher, R. H., *Computational Fluid Mechanics and Heat Transfer*, Hemisphere, New York, 1984.

[47]Buelow, P. E., Ievalts, J. O., and Tannehill, J. C., "Comparison of Three-Dimensional Nonequilibrium PNS Codes," AIAA Paper 90-1572, June 1990.